Organic & Biomolecular Chemistry

PAPER

View Article Online
View Journal | View Issue

Check for updates

Cite this: *Org. Biomol. Chem.*, 2018, **16**, 7871

Dynamic Diels–Alder reactions of maleimide–furan amphiphiles and their fluorescence ON/OFF behaviours†

Fen Li, Xiaohui Li and Xin Zhang *

The occurrence of dynamic covalent reactions only requires relatively low activation energy, which allows both the forward and reverse reactions to proceed under mild conditions. Here, we report the design and synthesis of amphiphilic maleimide–furan adducts, where hydrophobic maleimide-based and hydrophilic furan-based moieties were connected by reversible dynamic covalent bonds. The Diels–Alder addition reactions of maleimide–furan adducts are simple, efficient, clean, and reversible without catalysts and side reactions, and occur under mild conditions. Single crystal X-ray diffraction revealed that the length of the dynamic covalent bonds is 1.56 Å, which is longer and weaker than for normal covalent bonds. The cleavage and reformation process of the dynamic covalent bonds was monitored by ^{1}H NMR and fluorescence spectroscopy. ^{1}H NMR spectroscopy revealed that the furan moieties of these new maleimide–furan amphiphiles can be exchanged in mixing systems due to dynamic Diels–Alder reactions; thus, two new maleimide–furan compounds can be transformed into each other. The maleimide–furan amphiphiles displayed reversible fluorescence ON/OFF behaviours and interesting H-bonding driven supramolecular assembly.

Received 9th August 2018,
Accepted 2nd October 2018

DOI: 10.1039/c8ob01944d

rsc.li/obc

Published on 02 October 2018. Downloaded by Tulane University on 12/20/2018 2:52:16 AM.

Introduction

Dynamic covalent reactions enable chemists to design and create a wide variety of small molecular, macromolecular and supramolecular structures including covalent organic frameworks, molecular knots and macrocycles, which have demonstrated diverse applications such as renewable and recyclable, and self-healing materials, gas storage, catalysis, functional polymers and biomaterial sensors.[1] The most interesting feature of dynamic covalent chemistry is the dynamic reversibility of the formation and cleavage of covalent bonds, which combines the dynamic properties of supramolecular chemical bonds and robustness of covalent bonds.[2] The dynamic covalent bond reversibility enables continual exchange of moieties in multimolecular mixing systems under thermodynamic equilibrium conditions. Dynamic covalent reactions include many classic chemistry reactions such as transesterifications,[3] Cannizzaro or aldol exchange and condensations,[4] boronate ester condensations[5] and olefin metathesis reaction,[6] disulfide bond formation,[7] imine condensation[8] and Diels–Alder cycloaddition.[9]

Maleimides are one significant class of unsaturated cyclic imides and electron-poor dienophiles.[10] The strong electron-withdrawing properties of maleimide groups effectively decrease the lowest unoccupied molecular orbital energy, and thus promote Diels–Alder addition reactions with electron-rich dienes such as cyclopentadienes or furans.[11] In addition, maleimides are also easily attacked by thiols, amines, and dienes through the Michael reaction.[12] Thus, maleimides have been recognized as promising scaffolds and molecules to prepare functional polymers, hydrogels, and high performance thermosetting bismaleimide resins.[13] We have had a long-standing interest in the synthesis and optical behaviours of functional dyes and chromophores.[14] Recently, Ghosh *et al.* have reported the synthesis of chromophore-conjugated amphiphiles including naphthalene-diimide derivatives, and found that the high fluorescence properties remained in the assembly states.[1c,15] Beuerle *et al.* reported the synthesis of dynamic covalent cage compounds based on boronate ester condensations.[16] Zhang W. and Jin *et al.* reported an imine-linked 2D covalent monolayer through dynamic imine condensation between terephthaldehyde and 1,3,5-trihexyl-2,4,6-tris(4-aminophenyl)benzene at the air/water interface.[17] Here, we report the synthesis of a new class of amphiphilic maleimide–furan adducts, where the hydrophobic and hydrophilic parts are connected by dynamic

School of Chemical Engineering and Technology, Tianjin University, Tianjin, 300072, China. E-mail: xzhangchem@tju.edu.cn

† Electronic supplementary information (ESI) available: Experimental procedures and characterization spectra. CCDC 1851016. For ESI and crystallographic data in CIF or other electronic format see DOI: 10.1039/c8ob01944d

Published on 02 October 2018. Downloaded by Tulane University on 12/20/2018 2:52:16 AM.

covalent bonds formed through the Diels–Alder reaction. In particular, we demonstrate that the efficient, clean, and reversible Diels–Alder addition reactions of maleimide–furan adducts lead to reversible optical behaviours.

Results and discussion

In this work, we synthesized carbazole-containing maleimide **1** and amphiphilic maleimide–furan adducts **2**, **3**, and **4** by 7-step reactions (Schemes 1 and 2 and the ESI†). The chemical structures of **2** and **3** consist of hydrophobic maleimide-based and hydrophilic furan-based moieties (Fig. 1a). The hydrophobic and hydrophilic parts are connected by dynamic covalent bonds (Fig. 1a). The precursor *N*-nitrobenzene carbazole was synthesized by the Ullmann reaction from carbazole and 4-chloronitrobenzene, then reduced by hydrazine hydrate in the presence of Pd/C (10 wt%) as a catalyst.[18] The resulting aromatic amine was reacted with maleic anhydride, and then a cyclization reaction was performed in acetic anhydride with sodium acetate to give the *N*-phenylcarbazole maleimide **1**. The hydrophilic furan derivative with an oligoethylene glycol chain was synthesized by the Sonogashira reaction of 3-(2-(2-ethoxyethoxy)ethoxy)-1-propyne with 4-bromo-2-furaldehyde,

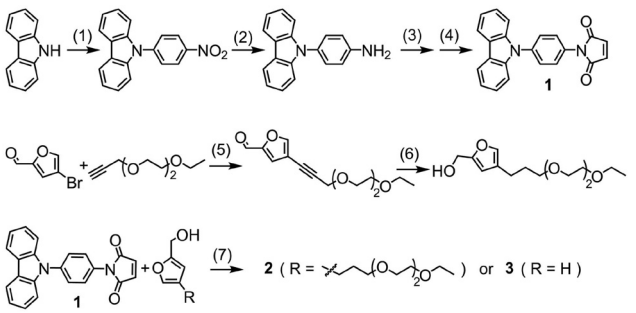

Scheme 1 Synthetic route to *N*-phenylcarbazole maleimide **1**, amphiphilic **2** and **3**. Reagents and conditions: (1) 4-Nitrochlorobenzene, K_2CO_3, dimethyl sulfoxide, 150 °C, 28%; (2) Pb/C (10 wt%), hydrazine hydrate (80 wt%), ethanol, 80 °C, 98%; (3) maleic anhydride, dichloromethane, r.t., 95%; (4) acetic anhydride, sodium acetate anhydrous, 80 °C, 47%; (5) copper(I) iodide, tetrakis(triphenylphosphine) palladium, anhydrous triethylamine, 70 °C, 33%; (6) Pd/C (10 wt%), acetic acid, $NaBH_4$, alcohol, r.t., 53%; (7) chloroform, acetonitrile, 70 °C, 41% and 27% for **2** and **3**.

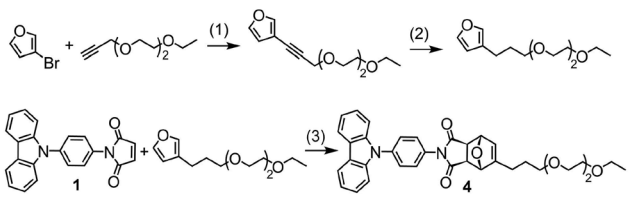

Scheme 2 Synthetic route to maleimide–furan adduct **4**. Reagents and conditions: (1) Copper(I) iodide, tetrakis(triphenylphosphine) palladium, anhydrous triethylamine, 70 °C, 39%; (2) Pd/C (10 wt%), acetic acid, $NaBH_4$, alcohol, r.t., 75%; (3) chloroform, acetonitrile, 70 °C, 69%.

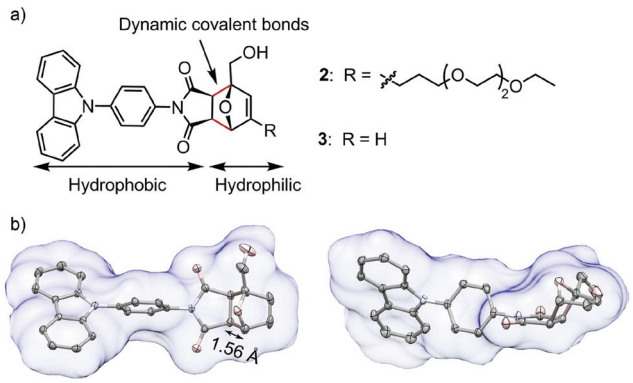

Fig. 1 (a) Chemical structures of amphiphilic maleimide–furan adducts **2** and **3**. Dynamic covalent bonds connecting hydrophobic and hydrophilic moieties are indicated in red. (b) Molecular structure (ORTEP) of **3** determined by single-crystal X-ray diffraction, top view (left) and side view (right). Thermal ellipsoids are drawn at 50% probability level. All hydrogen atoms are omitted for clarity.

and subsequently reduced using $NaBH_4$ and acetic acid, with Pd/C.[19] The final products **2** and **3** were obtained by the Diels–Alder reaction between *N*-phenylcarbazole maleimide **1** and furan derivatives in chloroform/acetonitrile at room temperature.

Maleimide–furan adducts **2** and **3** are new compounds. The chemical structures of **2** and **3** are fully characterized by ^{1}H and ^{13}C NMR spectroscopy, and high-resolution mass spectrometry (see the details in the ESI†). We further obtained the single crystal of **3** by slow evaporation of its dichloromethane/*n*-hexane solution. The X-ray crystal structure of **3** indicates 4 molecules in a unit cell and a monoclinic space group $P2(1)/n$. The *N*-phenyl group is twisted by 56.2° from the plane of the carbazole group (Fig. 1b). The X-ray diffraction results[20] demonstrated that the length of the dynamic covalent bonds connecting the hydrophobic and hydrophilic parts (Fig. 1b) is 1.56 Å, which are longer, and thus weaker than normal single bonds (1.54 Å).[21] Thus, the dynamic covalent bonds can easily be cleaved under appropriate conditions.

The UV/Vis absorption spectra of **1**, **2** and **3** show the same absorption peak at 295 nm in dichloromethane (Fig. 2a), which is assigned to the π–π* transition of the carbazole chromophore.[22] However, the fluorescence spectra of *N*-phenylcarbazole maleimide **1** and its adducts **2** and **3** are distinctly different. No fluorescence was observed for maleimide **1**. However, the adducts **2** and **3** displayed high fluorescence at 330–400 nm (Fig. 2b and c). The fluorescence quantum yields of **2** and **3** were found to be 0.41 and 0.36 with the same fluorescence lifetime of 4.6 ns in dichloromethane (Fig. 2b inset and Fig. 2c inset).

As described in the X-ray crystal structures, the dynamic covalent bonds of maleimide–furan adducts break easily. ^{1}H NMR spectroscopy monitored the cleavage process of dynamic covalent bonds through a retro-Diels–Alder addition at elevated temperature (Fig. 3). During the retro-Diels–Alder addition of **3** at 80–100 °C in toluene at 0.061 M, the NMR

 This journal is © The Royal Society of Chemistry 2018

Published on 02 October 2018. Downloaded by Tulane University on 12/20/2018 2:52:16 AM.

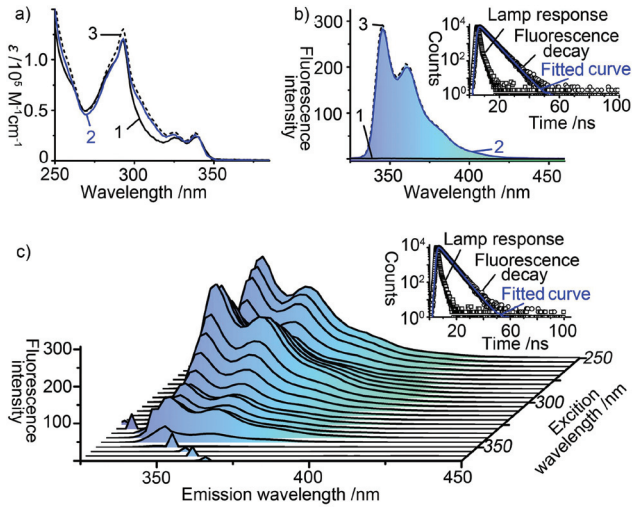

Fig. 2 (a) UV/Vis absorption spectra of **1**, **2** and **3** in dichloromethane. (b) Fluorescence spectra of **1**, **2** and **3** in dichloromethane. $c = 2 \times 10^{-5}$ M. Inset: Fluorescence decay of **3** in dichloromethane. Fluorescence lifetime was found to be 4.6 ns. Excitation and emission wavelengths are 295 nm and 345 nm. [**3**] = 2×10^{-5} M. (c) Three-dimensional excitation–emission fluorescence spectra of **2**. Inset: Fluorescence decay of amphiphilic **2** in dichloromethane. Fluorescence lifetime was found to be 4.6 ns. Excitation and emission wavelengths are 295 nm and 345 nm. [**1**] = 2×10^{-5} M.

peaks of the protons of **3** at δ 6.63–6.74 ppm (H_b and H_c) and δ 5.46–5.48 ppm (H_a) gradually decrease, and the NMR peak of the protons of **1** at δ 6.94 ppm (H_d) appears and gradually increases (Fig. 4a). For this process, the fluorescence intensity of **3** gradually decreases, and finally disappears (Fig. 3b). The fluorescence intensity changes during the retro-Diels–Alder addition of **3** well agree with the reaction monitoring by NMR spectroscopy (Fig. 3b, inset). Thus, fluorescence spectroscopy can monitor the cleavage extent of dynamic covalent bonds.

After cooling the above reaction systems to room temperature, the resulting *N*-phenylcarbazole maleimide **1** and furan derivative start to perform the Diels–Alder reaction in $CDCl_3$ at 0.055 M, and reform **2** or **3** (Fig. 4), and dynamic covalent bonds were reformed in **2** or **3**. The reformation process of the dynamic covalent bonds was monitored by ^{1}H NMR spectroscopy. The NMR peaks of the protons of **1** at 6.94 ppm (H_d) and furan derivatives at δ 6.35–6.30 ppm ($H_{b'}$ and $H_{c'}$) gradually decrease. The NMR peaks of the protons of **3** appear at δ 6.62–6.70 ppm (H_b and H_c) and 5.43 ppm (H_a) and gradually increase as the room temperature Diels–Alder reaction proceeds (Fig. 4a). It should be noted that the Diels–Alder reaction first forms two isomers:[23,24] *endo* and *exo* isomers (Fig. S9 and S12†). The *exo* isomer is thermodynamically stable, and the *endo* isomer is kinetically favored. As the reaction proceeds, the kinetically favored *endo* isomer gradually disappears, and the thermodynamically stable *exo* isomer becomes dominant. Thus, we finally obtained a pure *exo* isomer (Fig. 1, Fig. S10

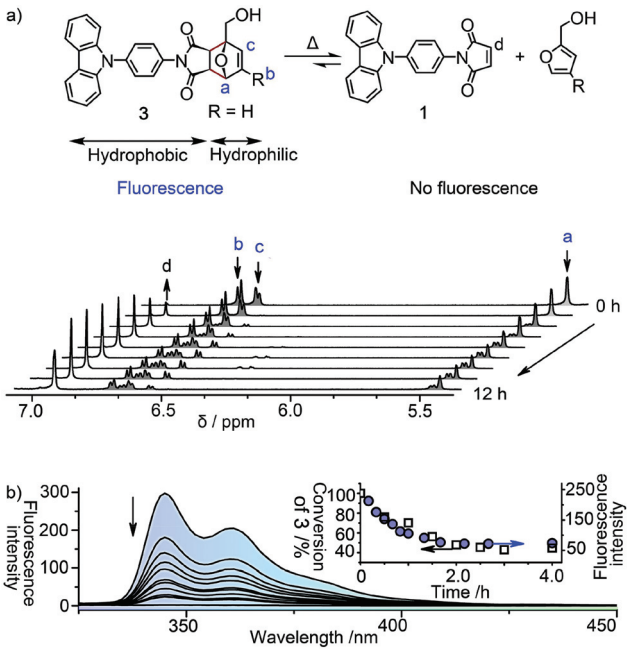

Fig. 3 (a) Cleavage of dynamic covalent bonds (shown in red) by the retro-Diels–Alder reaction in toluene at 80–100 °C and ^{1}H NMR spectral changes during the retro-Diels–Alder reaction of **3**. (b) Fluorescence spectra during the retro-Diels–Alder reaction of **3** from 0 h (top) to 12 h (bottom). Inset: Retro-Diels–Alder reaction of **3** monitored by ^{1}H NMR spectroscopy according to the changes at δ = 5.44–5.49 ppm, and by fluorescence spectroscopy according to intensity changes at 345 nm.

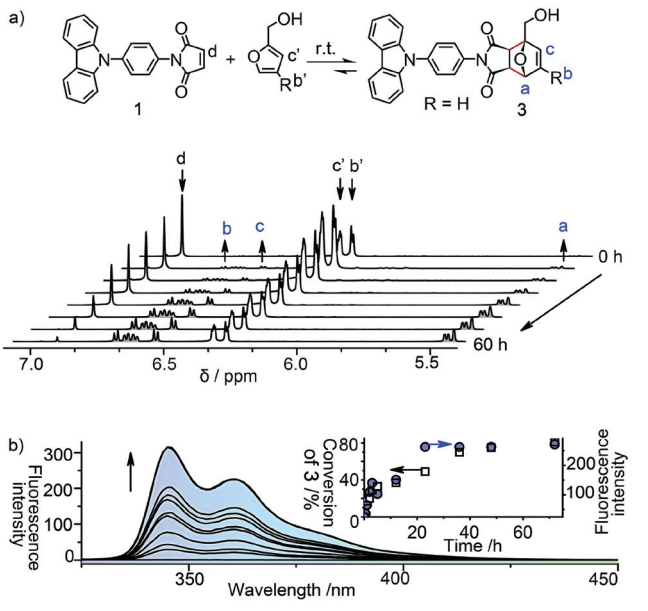

Fig. 4 (a) Reformation of dynamic covalent bonds (shown in red) by the Diels–Alder reaction in chloroform at room temperature, and ^{1}H NMR spectral changes during **3** reformation by the Diels–Alder reaction. (b) Fluorescence spectra during **3** reformation by the Diels–Alder reaction at room temperature from 0 h (bottom) to 60 h (top). Inset: Diels–Alder addition reaction of **3** reformation monitored by ^{1}H NMR spectroscopy according to the changes at δ = 5.44–5.49 ppm, and by fluorescence spectroscopy according to intensity changes at 345 nm.

Published on 02 October 2018. Downloaded by Tulane University on 12/20/2018 2:52:16 AM.

and S13†). The fluorescence of **2** or **3** appears and gradually increases as the reaction proceeds (Fig. 4b). Thus, the Diels–Alder reaction is a typical fluorigenic reaction. The fluorescence intensity changes well agree with the reaction monitoring from ^{1}H NMR spectroscopy (Fig. 4b, inset). Thus, fluorescence changes reflect the reformation or repair extent of dynamic covalent bonds through Diels–Alder addition. Furthermore, ^{1}H NMR spectroscopy revealed that the Diels–Alder addition reactions of maleimide–furan adducts are simple, efficient, clean, and reversible without catalysts and side reactions.

The Diels–Alder reactions are dynamic. We further studied the exchange of furan moieties during the dynamic reaction process (Fig. 5). **2** and furfuryl alcohol were dissolved in deuteroacetonitrile (CD_3CN), and the mixture was heated at 75 °C with stirring. The reaction was monitored by NMR spectroscopy. The ^{1}H NMR peaks of the protons of **3** at δ 6.62–6.70 ppm (H_b and H_c) and δ 5.43 ppm (H_a) and oligoethylene glycol-containing furan at δ 6.18 ($H_{g'}$) and δ 4.52–4.57 ppm ($H_{h'}$) gradually increase as dynamic exchange reaction proceeds (Fig. 5). At the same time, the peaks of the protons of **2** at δ 6.23 ppm (H_g) and furfuryl alcohol at δ 6.21–6.36 ppm ($H_{b'}$ and $H_{c'}$) decrease. These results reveal that **2** is transformed into **3** by the exchange of furan moieties. The dynamic Diels–Alder reaction reversibility enables continual exchange of furan moieties in the **2** and **3** mixing systems under thermodynamic equilibrium conditions, where the oligoethylene glycol-containing furan moiety was exchanged by furfuryl alcohol due to reducing steric hindrance.

Molecularly dissolved **2** in THF is highly fluorescent with emission maxima at 345 nm and 360 nm. Upon adding deionized water into the THF solution of **2**, the fluorescence of monomer **2** decreases gradually, and new emission peaks appear and increase at 402 nm and 425 nm with a red shift of 57–67 nm (Fig. 6c). We attributed the new broad fluorescence peaks to the assembly occurring of amphiphilic **2** in aqueous solution.

We subsequently explore the assembly behaviour of **2** in aqueous solution. The aggregates of **2** were prepared as follows: the amphiphilic **2** was first dissolved in THF, and the same volume of deionized water was then slowly added. Then,

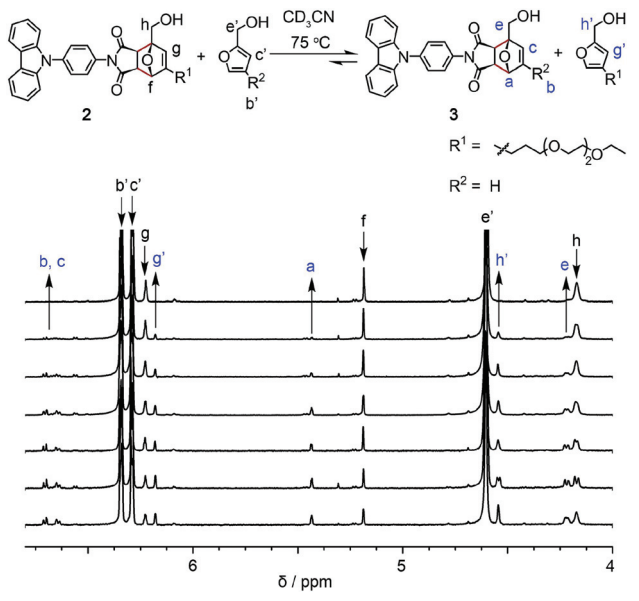

Fig. 5 Exchange of furan moieties between **2** and **3** monitored by ^{1}H NMR spectroscopy during the dynamic Diels–Alder reaction in CD_3CN at 75 °C. [**2**] = 0.05 M. Reaction time = 0, 3, 6, 12, 24, 48, 72 h from top to bottom.

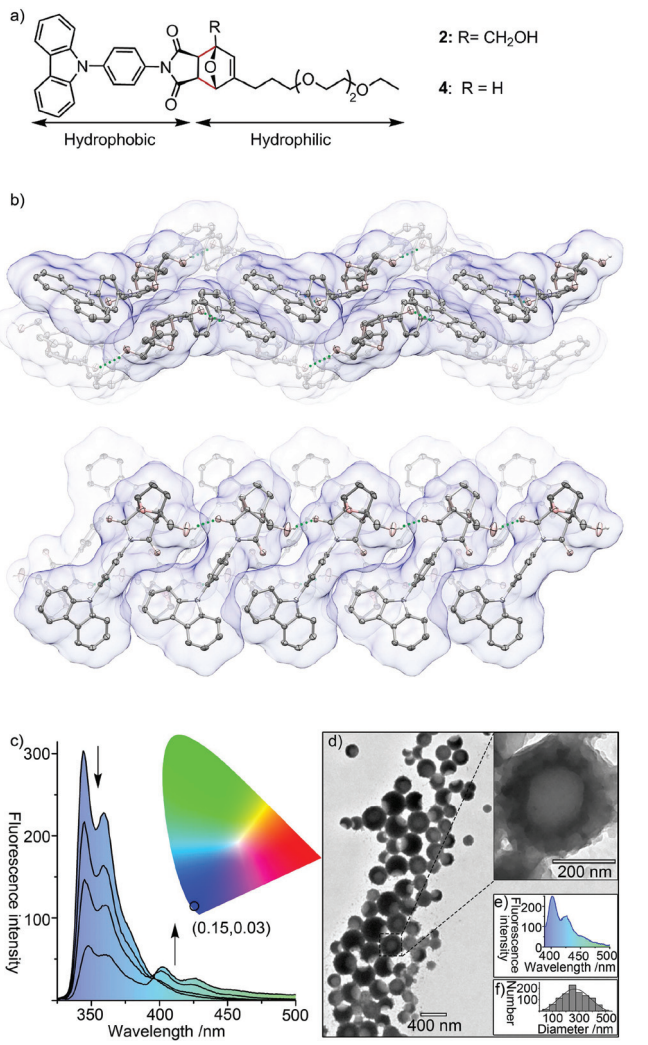

Fig. 6 (a) Chemical structures of maleimide–furan adducts **2** and **4**. (b) H-bonding (shown in green) driven crystal packing structure of maleimide–furan adduct **3**, side view (top) and top view (bottom). (c) Fluorescence spectra of **2** with increasing deionized water contents in THF from 80% (top) to 95% (bottom). Inset: CIE 1931 chromaticity diagram of the aggregtes in water-containing THF (95%, v/v). [**2**] = 2.0 × 10^{-5} M. Excitation wavelength is 295 nm. (d) TEM images of **2** aggregates prepared from the aqueous solution and stained with uranyl acetate. The inset shows one magnified TEM image of one typical vesicular aggregate. (e) Fluorescence spectrum of **2** vesicular aggregates. (f) Size distribution of the vesicular aggregates obtained from TEM measurements. [**2**] = 2 × 10^{-4} M.

This journal is © The Royal Society of Chemistry 2018

Published on 02 October 2018. Downloaded by Tulane University on 12/20/2018 2:52:16 AM.

THF was evaporated slowly at room temperature to give the aqueous solution of **2** at a concentration of 2×10^{-4} M. The solution was kept at room temperature to form the stable and energy-minimized aggregates for transmission electron microscopy (TEM) measurements. TEM results indicate that spherical hollow vesicles were formed from amphiphilic **2** with an average diameter of 270 nm (Fig. 6d and Fig. S22†). Dynamic light scattering (DLS) measurements (Fig. S23†) revealed that the average size of these vesicular aggregates is 380 nm in deionized water, which is slightly larger than the TEM results. This is due to the fact that DLS and TEM were performed in solution and dried state of the samples, respectively.[14a]

The vesicular aggregates of **2** emit blue fluorescence at 400–450 nm with CIE color coordinates (0.15, 0.03) (Fig. 6c inset). We further measured the fluorescence spectroscopic changes by increasing the concentration of **2** (Fig. S21†). The plot of fluorescence intensity *versus* concentration shows a critical turning point, suggesting that the critical aggregation concentration of the formation of vesicular aggregates of **2** is 1.1×10^{-5} M in deionized water. To explore the assembly mechanism of amphiphilic **2**, we analysed the crystal structure of maleimide–furan adduct **3** (Fig. 6b). In the crystal packing structure of **3**, intermolecular C═O···H–O hydrogen bonds are formed with a bond length of 2.03 Å (shown in green in Fig. 6b). According to the crystal packing structure (Fig. 6b), the H-bonding interaction occurs in the hydrophobic phase, which protects H-bonding formation and prevents its interaction with solvents. Similar examples can be found for the H-bonding driven aggregate formation of natural chlorophyll analogues in water.[25] Therefore, the main driving force of the assembly of amphiphilic **2** in aqueous solution is H-bonding interaction and hydrophobic interaction. The vesicular aggregates of **2** are fluorescent in aqueous solution with an emission maximum at 402 nm (Fig. 6e).

To further confirm the H-bonding driving force[14] for the aggregation of amphiphilic **2**, we synthesized amphiphilic maleimide–furan adduct **4** (Scheme 2 and Fig. 6a). The 3-(3-{2-[2-(ethoxy)ethoxy]ethoxy}propyl)furan was synthesized by the Sonogashira reaction of 3-(2-(2-ethoxyethoxy)ethoxy)-1-propyne with 3-bromofuran, and subsequently reduced using $NaBH_4$ and acetic acid, with Pd/C. Finally, the adduct **4** was synthesized by the Diels–Alder reaction from the corresponding furan derivative and *N*-phenylcarbazole maleimide **1** in chloroform/acetonitrile at room temperature. The maleimide–furan adduct **4** shows a UV-vis absorption peak at 295 nm and fluorescence emission at 345 nm with a fluorescence lifetime of 4.6 ns and quantum yields of 0.37, which are similar to the optical properties of the adducts **2** and **3**. The detailed optical parameters of these compounds **1**, **2**, **3** and **4** are listed in Table 1.

The chemical structures of **2** and **4** possess the same hydrophobic moiety and the hydrophilic oligoethylene glycol-containing furan moiety. The only difference is that no CH_2OH group exists in the furan moiety for **4**. Thus, no H-bonding interaction can form for **4** assembly. We attempt to prepare the aggregates of **4** in aqueous solution according to the preparation procedure of **2**. However, no highly ordered aggregates were observed by TEM. Amphiphilic maleimide–furan adduct **4** cannot assemble into well-defined aggregates in aqueous solution due to the absence of H-bonding interaction. These results further confirm the H-bonding driven supramolecular assembly of maleimide–furan adducts **2** and **3**. In general, supramolecular vesicular aggregates can be destroyed after high temperature thermal treatment.[14a] We found that our vesicular aggregates were reformed and self-healed after thermal treatment at 90 °C for 2 h (Fig. S24†). We attributed this self-healing behaviour to the reformation of dynamic covalent bonds between hydrophobic and hydrophilic moieties. An in-depth study on the self-healing performance and related fluorescence behaviours is under way.

Table 1 UV-vis absorption and fluorescence spectral data of **1**, **2**, **3** and **4**

	UV-vis absorption		Fluorescence		
	λ_{ab} (nm)	ϵ ($\times 10^5$ M^{-1} cm^{-1})	λ_{em} (nm)	Φ	τ (ns)
1	295	1.19	—	—	—
2	295	1.21	345	0.41	4.6
3	295	1.31	345	0.36	4.6
4	293	1.05	345	0.37	4.6

Conclusions

In summary, we designed and synthesized carbazole-containing maleimide **1** and amphiphilic maleimide–furan adducts **2**, **3** and **4**. The chemical structure of **2** consists of hydrophobic maleimide-based and hydrophilic furan-based moieties connected by dynamic covalent bonds. Dynamic Diels–Alder reactions of maleimide–furan adducts lead to reversible fluorescence ON/OFF behaviours as revealed by ^{1}H NMR and fluorescence spectroscopy. The exchange experiment of the furan moieties of these new maleimide–furan amphiphiles confirms the dynamic nature of this Diels–Alder reaction. Maleimide–furan **2** can be transformed into **3** by continual exchange of furan moieties in mixing systems during the dynamic reaction. The maleimide–furan adducts **2** and **3** displayed H-bonding driven suparmolecular assembly. Fluorescent vesicular aggregates were formed from maleimide–furan amphiphile **2** in deionized water. Our results will encourage the development of dynamic Diels–Alder reactions and their potential properties and applications.

Experimental section

Maleimide–furan adduct 2

N-Phenylcarbazole maleimide **1** (0.17 g, 0.5 mmol) and [4-(3-{2-[2-(ethoxy)ethoxy]ethoxy}propyl)furan-2-yl]methanol (0.16 g, 0.6 mmol) were dissolved in chloroform (5 mL) and aceto-

Published on 02 October 2018. Downloaded by Tulane University on 12/20/2018 2:52:16 AM.

nitrile (5 mL) under N_2. The mixture was heated at 70 °C with stirring for 24 h. The mixture was washed with water and extracted by dichloromethane (10 mL). The organic layer was collected and dried over anhydrous magnesium sulfate. After concentrating under reduced pressure, the crude product was purified by silica gel column chromatography (ethyl acetate/petroleum ether = 1/1, v/v) giving a white solid (0.20 g, 41%). ^{1}H NMR (400 MHz, $CDCl_3$): δ = 8.14 (d, J = 7.7 Hz, 2H), 7.62 (dd, J = 60.9, 8.6 Hz, 4H), 7.47 (d, J = 8.1 Hz, 2H), 7.42 (t, J = 7.4 Hz, 2H), 7.30 (t, J = 7.2 Hz, 2H), 6.23 (s, 1H), 5.20 (s, 1H), 4.17 (d, J = 6.0 Hz, 2H), 3.81–3.43 (m, 12H), 3.23 (s, 2H), 2.73 (s, 1H), 2.38 (t, J = 7.5 Hz, 2H), 1.93–1.77 (m, 2H), 1.22 (t, J = 7.0 Hz, 3H). ^{13}C NMR (100 MHz, $CDCl_3$): δ = 175.32, 175.24, 152.57, 140.55, 138.08, 130.35, 130.20, 127.96, 127.54, 126.12, 123.56, 120.38, 120.32, 109.78, 92.72, 83.76, 70.71, 70.65, 70.31, 69.86, 66.68, 61.20, 49.94, 49.72, 27.20, 24.27, 15.20. IR (cm^{-1}): 3463, 2865, 1774, 1704, 1599, 1515, 1478, 1451, 1387, 1356, 1317, 1228, 1181, 1103, 977, 927, 831, 750, 723. HRMS (ESI): m/z calculated for $C_{36}H_{38}N_2O_7$ $[M + Na]^+$: 633.2571, found: 633.2572.

Maleimide–furan adduct 3 was synthesized in the same manner as **2**, except for [4-(3-{2-[2-(ethoxy)ethoxy]ethoxy} propyl)furan-2-yl]methanol replaced with furfuryl alcohol (0.1 mL). The crude product was purified by silica gel column chromatography (ethyl acetate/petroleum ether = 1/1, v/v) to give a white solid (0.12 g, 27%). ^{1}H NMR (400 MHz, $CDCl_3$): δ = 8.14 (d, J = 7.7 Hz, 2H), 7.62 (dd, J = 59.6, 8.6 Hz, 4H), 7.46 (d, J = 8.1 Hz, 2H), 7.41 (t, J = 7.5 Hz, 2H), 7.30 (t, J = 7.3 Hz, 2H), 6.66 (dd, J = 29.5, 5.7 Hz, 2H), 5.43 (s, 1H), 4.21 (s, 2H), 3.20 (dd, J = 17.6, 6.6 Hz, 2H), 2.72 (s, 1H). ^{13}C NMR (100 MHz, $CDCl_3$): δ = 175.08, 174.97, 140.61, 138.58, 138.18, 137.21, 130.22, 127.93, 127.57, 126.13, 123.61, 120.37, 120.34, 109.77, 91.96, 81.52, 60.87, 50.13, 48.29, 25.38. IR: 2372, 1776, 1700, 1599, 1544.17, 1517, 1478, 1453, 1404, 1363, 1338, 1316.94, 1301, 1282, 1232, 1207, 1194, 1056, 1019, 757. HRMS (ESI): m/z calculated for $C_{27}H_{20}N_2O_4$ $[M + Na]^+$: 495.1315, found 459.1315.

Maleimide–furan adduct 4 was synthesized in the same manner as **2**, except for [4-(3-{2-[2-(ethoxy)ethoxy]ethoxy} propyl)furan-2-yl]methanol replaced with 3-(3-{2-[2-(ethoxy) ethoxy]ethoxy}propyl)furan (0.15 g, 0.6 mmol). The crude product was purified by silica gel column chromatography (ethyl acetate/petroleum ether = 3/2, v/v) to give a pale yellow solid (0.2 g, yield 69%). ^{1}H NMR (400 MHz, $CDCl_3$): δ = 8.17–8.10 (m, 2H), 7.72–7.53 (m, 4H), 7.49–7.45 (m, 2H), 7.36 (m, 4H), 6.12 (q, J = 1.7 Hz, 1H), 5.37 (s, 1H), 5.20 (s, 1H), 3.73–3.48 (m, 12H), 3.10 (dd, J = 19.2, 6.6 Hz, 2H), 2.37 (t, J = 7.6 Hz, 2H), 1.91–1.76 (m, 2H), 1.22 (t, J = 7.0 Hz, 3H). ^{13}C NMR (100 MHz, $CDCl_3$): δ = 175.63, 175.47, 152.03, 140.59, 137.92, 130.46, 128.71, 128.04, 127.51, 126.10, 123.54, 120.35, 120.26, 109.80, 83.85, 82.41, 77.24, 70.64, 70.34, 70.32, 69.86, 66.68, 49.40, 47.34, 27.29, 24.10, 15.20. IR (cm^{-1}): 2863, 1707, 1600, 1515, 1478, 1451, 1385, 1356, 1334, 1229, 1179, 1104, 1016, 936, 870, 825, 750, 723. HRMS (ESI): m/z calculated for $C_{35}H_{36}N_2O_6$ $[M + Na]^+$: 603.2466, found: 603.2466.

Cleavage and reformation of dynamic covalent bonds monitored by ^{1}H NMR and fluorescence spectroscopy

The adduct **3** (41.1 mg, 0.061 mmol) was dissolved in toluene (1 mL), and heated at 100 °C with stirring. 40 μL of the above toluene reaction solution of **3** was placed in a NMR tube at specific time intervals. This sample solution in the NMR tube was dried *in vacuo* for over 24 h. Deuterochloroform ($CDCl_3$) (0.5 mL) was added in each NMR sample tube for NMR measurements. 25 μL of the $CDCl_3$ solution of **3** was transferred from each NMR sample tube into 20 mL bottles, and diluted to 10 mL with dichloromethane for fluorescence measurements.

Exchange of furan moieties between 2 and 3

Compound **2** (30.5 mg, 0.05 mmol) was dissolved in deuteroacetonitrile (CD_3CN) (1 mL), and then furfuryl alcohol (5 mg, 0.05 mol) was added. The mixture solution was heated at 75 °C with stirring. 20 μL of the above solution was taken and placed in a NMR tube at specific time intervals. Deuterochloroform ($CDCl_3$) (480 μL) was then added respectively in each NMR sample tube for NMR measurements.

Conflicts of interest

There are no conflicts to declare.

Acknowledgements

The authors acknowledge the financial support of the National Natural Science Foundation of China (Grant No. 21674079) and the Tianjin Research Program of Application Foundation and Advanced Technology (No. 15JCYBJC20400), and acknowledge Xiaoxin Zhao for the kind help with NMR measurements.

Notes and references

1 (*a*) J. M. Lehn, *Chem. Soc. Rev.*, 2007, **36**, 151–160; (*b*) S. J. Rowan, S. J. Cantrill, G. R. L. Cousins, J. K. M. Sanders and J. F. Stoddart, *Angew. Chem., Int. Ed.*, 2002, **41**, 899–952; (*c*) M. R. Molla and S. Ghosh, *Phys. Chem. Chem. Phys.*, 2014, **16**, 26672–26683; (*d*) H. J. Kim, T. Kim and M. Lee, *Acc. Chem. Res.*, 2011, **44**, 72–82; (*e*) T. Maeda, H. Otsuka and A. Takahara, *Prog. Polym. Sci.*, 2009, **34**, 581–604; (*f*) A. G. Slater and A. I. Cooper, *Science*, 2015, **348**, aaa8075; (*g*) C. S. Diercks and O. M. Yaghi, *Science*, 2017, **355**, eaal1585.

2 (*a*) R. J. Wojtecki, M. A. Meador and S. J. Rowan, *Nat. Mater.*, 2011, **10**, 14–27; (*b*) P. T. Corbett, J. Leclaire, L. Vial, K. R. West, J. L. Wietor, J. K. M. Sanders and S. Otto, *Chem. Rev.*, 2006, **106**, 3652–3711; (*c*) F. Beuerle and B. Gole, *Angew. Chem., Int. Ed.*, 2018, **57**, 4850–4878; (*d*) F. Beuerle and B. Gole, *Angew. Chem., Int. Ed.*, 2018, **57**, 4850–4878; (*e*) G. Zhang and M. Mastalerz, *Chem. Soc. Rev.*, 2014, **43**,

 This journal is © The Royal Society of Chemistry 2018

Published on 02 October 2018. Downloaded by Tulane University on 12/20/2018 2:52:16 AM.

1934–1947; (*f*) T. Hasell and A. I. Cooper, *Nat. Rev. Mater.*, 2016, **1**, 16053; (*g*) S. Y. Ding and W. Wang, *Chem. Soc. Rev.*, 2013, **42**, 548–568.

3 (*a*) Y. Jin, C. Yu, R. J. Denman and W. Zhang, *Chem. Soc. Rev.*, 2013, **42**, 6634–6654; (*b*) N. Huang, P. Wang and D. Jiang, *Nat. Rev. Mater.*, 2016, **1**, 16068; (*c*) R. P. Bisbey and W. R. Dichtel, *ACS Cent. Sci.*, 2017, **3**, 533–543.

4 (*a*) S. I. Kawano, M. Kato, S. Soumiya, M. Nakaya, J. Onoe and K. Tanaka, *Angew. Chem., Int. Ed.*, 2018, **57**, 167–171; (*b*) W. Dai, F. Shao, J. Szczerbiński, R. McCaffrey, R. Zenobi, Y. Jin, A. D. Schlüter and W. Zhang, *Angew. Chem., Int. Ed.*, 2016, **55**, 213–217; (*c*) P. Mal, D. Schultz, K. Beyeh, K. Rissanen and J. R. Nitschke, *Angew. Chem., Int. Ed.*, 2008, **47**, 8297–8301.

5 (*a*) S. Lascano, K. D. Zhang, R. Wehlauch, K. Gademann, N. Sakai and S. Matile, *Chem. Sci.*, 2016, **7**, 4720–4724; (*b*) W. L. A. Brooks and B. S. Sumerlin, *Chem. Rev.*, 2016, **116**, 1375–1397; (*c*) R. Deng, M. J. Derry, C. J. Mable, Y. Ning and S. P. Armes, *J. Am. Chem. Soc.*, 2017, **139**, 7617–7623.

6 (*a*) J. P. Moerdyk and C. W. Bielawski, *Nat. Chem.*, 2012, **4**, 275–280; (*b*) C. K. Chu, T. P. Lin, H. Shao, A. L. Liberman-Martin, P. Liu and R. H. Grubbs, *J. Am. Chem. Soc.*, 2018, **140**, 5634–5643.

7 (*a*) Y. Altay, M. Tezcan and S. Otto, *J. Am. Chem. Soc.*, 2017, **139**, 13612–13615; (*b*) A. Takahara, R. Goseki and H. Otsuka, *Angew. Chem., Int. Ed.*, 2017, **56**, 2016–2021.

8 (*a*) Y. Jin, Y. Zhu and W. Zhang, *CrystEngComm*, 2013, **15**, 1484–1499; (*b*) M. E. Belowich and J. F. Stoddart, *Chem. Soc. Rev.*, 2012, **41**, 2003–2024; (*c*) J. L. Segura, M. J. Mancheño and F. Zamora, *Chem. Soc. Rev.*, 2016, **45**, 5635–5671.

9 (*a*) A. Gandini, *Prog. Polym. Sci.*, 2013, **1**, 1–29; (*b*) N. Wedler-Jasinski, T. Lueckerath, H. Mutlu, A. S. Goldmann, A. Walther, M. H. Stenzel and C. Barner-Kowollik, *Chem. Commun.*, 2017, **53**, 157–160.

10 Y. Heo and H. A. Sodano, *Adv. Funct. Mater.*, 2014, **24**, 5261–5268.

11 G. Delaittre, N. K. Guimard and C. Barner-Kowollik, *Acc. Chem. Res.*, 2015, **48**, 1296–1307.

12 Z. Huang, J. Zhao, Z. Wang, F. Meng, K. Ding, X. Pan, N. Zhou, X. Li, Z. Zhang and X. Zhu, *Angew. Chem., Int. Ed.*, 2017, **56**, 13612–13617.

13 T. Himiyama, N. Taniguchi, S. Kato, A. Onoda and T. Hayashi, *Angew. Chem., Int. Ed.*, 2017, **56**, 13618–13622.

14 (*a*) X. Zhang, S. Rehm, M. M. Safont-Sempere and F. Würthner, *Nat. Chem.*, 2009, **1**, 623–629; (*b*) X. Zhang, Z. C. Li, K. B. Li, S. Lin, F. S. Du and F. M. Li, *Prog. Polym. Sci.*, 2006, **31**, 893–948; (*c*) D. Görl, X. Zhang, V. Stepanenko and F. Würthner, *Nat. Commun.*, 2015, **6**, 7009.

15 (*a*) P. Rajdev, S. Chakraborty, M. Schmutz, P. Mesini and S. Ghosh, *Langmuir*, 2017, **33**, 4789–4795; (*b*) A. Sikder, A. Das and S. Ghosh, *Angew. Chem., Int. Ed.*, 2015, **54**, 6755–6760; (*c*) P. Pramanik, D. Ray, V. K. Aswal and S. Ghosh, *Angew. Chem., Int. Ed.*, 2017, **56**, 3516–3520.

16 (*a*) S. Klotzbach and F. Beuerle, *Angew. Chem., Int. Ed.*, 2015, **54**, 10356–10360; (*b*) A. Dhara and F. Beuerle, *Chem. – Eur. J.*, 2015, **21**, 17391–17396.

17 W. Dai, F. Shao, J. Szczerbiński, R. McCaffrey, R. Zenobi, Y. Jin, A. D. Schlüter and W. Zhang, *Angew. Chem., Int. Ed.*, 2016, **55**, 213–217.

18 X. Zhang, Z. C. Li, K. B. Li, F. S. Du and F. M. Li, *J. Am. Chem. Soc.*, 2004, **126**, 12200–12201.

19 A. T. Tran, V. A. Huynh, E. M. Friz, S. K. Whitney and D. B. Cordes, *Tetrahedron Lett.*, 2009, **50**, 1817–1819.

20 Crystallographic data for **3**: 0.4 × 0.3 × 0.1 mm^3, monoclinic, a = 13.4 Å, b = 10.0 Å, c = 15.8 Å, V = 2108.1 Å^3, space group $P2_1/c$, Z = 4, ρ_{calcd} = 1.38 g cm^{-3}, $\lambda_{(Mo(K\alpha)}$ = 0.71073 Å, T = 162 K, 7907 reflections, 3701 unique (2895 observed, R_{int} = 0.0308), R_1 = 0.0497, wR_2 = 0.1138, for 299 parameters and 0 restraints. The X-ray single crystal data of **3** deposited with the Cambridge Crystallographic Data Centre (CCDC 1851016†).

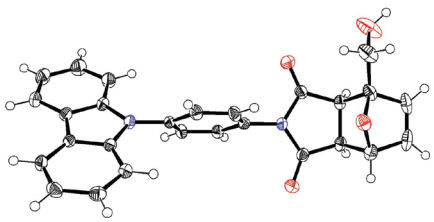

21 (*a*) B. R. Pool and J. M. White, *Org. Lett.*, 2000, **2**, 3505–3507; (*b*) A. K. H. Hirsch, P. Reutenauer, M. L. Moignan, S. Ulrich, P. J. Boul, J. M. Harrowfield, P. D. Jarowski and J. M. Lehn, *Chem. – Eur. J.*, 2014, **20**, 1073–1080; (*c*) O. Onaca, R. Enea, D. W. Hughes and W. Meier, *Macromol. Biosci.*, 2009, **9**, 129–139; (*d*) S. M. Taimoory, S. I. Sadraei, R. A. Fayoumi, S. Nasri, M. Revington and J. F. Trant, *J. Org. Chem.*, 2018, **83**, 4427–4440.

22 C. Kaewtong, G. Jiang, M. J. Felipe, B. Pulpoka and R. Advincula, *ACS Nano*, 2008, **2**, 1533–1542.

23 (*a*) V. Froidevaux, M. Borne, E. Laborbe, R. Auvergne, A. Gandinib and B. Boutevin, *RSC Adv.*, 2015, **5**, 37742–37754; (*b*) L. Rulísek, P. Šebek, Z. Havlas, R. Hrabal, P. Čapek and A. Svatos, *J. Org. Chem.*, 2005, **70**, 6295–6302.

24 R. C. Boutelle and B. H. Northrop, *J. Org. Chem.*, 2011, **76**, 7994–8002.

25 (*a*) M. Garzoni, M. B. Baker, C. M. A. Leenders, I. K. Voets, A. R. A. Palmans, E. W. Meijer and G. M. Pavan, *J. Am. Chem. Soc.*, 2016, **138**, 13985–13995; (*b*) S. Sengupta, D. Ebeling, S. Patwardhan, X. Zhang, H. Vona Berlepsch, C. Böttcher, V. Stepanenko, S. Uemura, C. Hentschel, H. Fuchs, F. C. Grozema, L. D. A. Siebbeles, A. R. Holzwarth, L. Chi and F. Würthner, *Angew. Chem., Int. Ed.*, 2012, **51**, 6378–6382.